Chinese Journal of Catalysis 38 (2017) 607–616

available at www.sciencedirect.com

ScienceDirect

journal homepage: www.elsevier.com/locate/chnjc

Article

Propene and CO oxidation on Pt/Ce-Zr-SO_4^{2-} diesel oxidation catalysts: Effect of sulfate on activity and stability

Lei Gu [a], Xiao Chen [a], Ying Zhou [b], Qiulian Zhu [b], Haifeng Huang [a,#], Hanfeng Lu [b,*]

[a] College of Environmental Engineering, Zhejiang University of Technology, Hangzhou 310014, Zhejiang, China

[b] Institute of Catalytic Reaction Engineering, College of Chemical Engineering, Zhejiang University of Technology, Hangzhou 310014, Zhejiang, China

ARTICLE INFO

Article history:
Received 8 December 2016
Accepted 4 January 2017
Published 5 March 2017

Keywords:
Diesel oxidation catalyst
Pt/Ce-Zr-SO_4^{2-} catalyst
Sulfur resistance
Catalytic oxidation

ABSTRACT

Platinum/cerium-zirconium-sulfate (Pt/Ce-Zr-SO_4^{2-}) catalysts were prepared by wetness impregnation. Catalytic activities were evaluated from the combustion of propene and CO. Sulfate (SO_4^{2-}) addition improved the catalytic activity significantly. When using Pt/Ce-Zr-SO_4^{2-} with 10 wt% SO_4^{2-}, the temperature for 90% conversion of propene and CO decreased by 75 °C compared with Pt/Ce-Zr. The conversion exceeded 95% at 240 °C even after 0.02% sulfur dioxide poisoning for 20 h. Temperature-programmed desorption of CO and X-ray photoelectron spectroscopy analyses revealed an improvement in Pt dispersion onto the Ce-Zr-SO_4^{2-} support, and the increased number of Pt particles built up more $Pt^{\delta+}$-$(SO_4^{2-})^{\delta-}$ couples, which resulted in excellent activity. The increased total acidity and new Brönsted acid sites on the surface provided the Pt/Ce-Zr-SO_4^{2-} with good sulfur resistance.

1. Introduction

Diesel vehicles are used widely because of their advantages of a high fuel efficiency, reliability, and durability. However, diesel-engine exhaust gases release various hazardous pollutants, such as carbon monoxide (CO), hydrocarbons (HC), nitrogen oxides (NO_x), particulate matter, and sulfur dioxide (SO_2). These substances are major sources of air pollution, such as haze fog, and are a threat to human and environmental health. Hence, regulations on exhaust-gas emissions from automotives are becoming stricter [1–5]. Diesel-vehicle catalyst systems that consist of diesel-oxidation catalysts (DOCs) [1,2], diesel particulate filters [6,7], and nitrous-oxide (NO_x) selective reduction catalysts (SCRs) [8,9] have been developed. These catalysts have been studied extensively to improve their activity and stability. DOCs have been used to convert unburned CO and hydrocarbons to carbon dioxide and water [10–13]. DOCs can also oxidize nitrogen monoxide to nitrogen dioxide, which is beneficial for de-NO_x activity of the fast SCR reaction and the oxidation of soot collected by the diesel particulate filters downstream [14,15].

Pt-based diesel-oxidation catalysts are used widely in DOC systems because of their high catalytic activity [16–18]. Ceria-zirconia solid solution is used as an excellent support because it combines a high oxygen storage/release capacity from the surface redox cycle Ce^{4+}/Ce^{3+}, and fine thermal stability caused by zirconium(IV) (Zr^{4+}) doping into the CeO_2 lattice [19]. A high dispersion of precious metal-like platinum is maintained by strong interaction of platinum-oxygen-cerium (Pt-O-Ce), which is termed the “anchor effect” [20]. However,

* Corresponding author. Tel: +86-571-88320767; E-mail: luhf@zjut.edu.cn
# Corresponding author. E-mail: hhf66@zjut.edu.cn
This work was supported by the National Natural Science Foundation of China (21506194, 21676255), the Provincial Natural Science Foundation of Zhejiang Province (LY16B070011), and the Commission of Science and Technology of Zhejiang Province (2017C33106, 2017C03007).
DOI: 10.1016/S1872-2067(17)62781-5| http://www.sciencedirect.com/science/journal/18722067 | Chin. J. Catal., Vol. 38, No. 3, March 2017

DOC catalysts are problematic in that the catalysts operate at low temperatures because the diesel exhaust gas temperature is significantly lower than that of the gasoline exhaust and is deactivated in the presence of SO_2 [21,22]. Consequently, oxidation catalysts are required urgently to improve the low-temperature activity and sulfur poisoning resistance in DOC systems.

Acidic oxide addition (such as sulfate) [23–27] can improve the low-temperature oxidation activity of catalysts remarkably. Gu et al. [23] showed that SO_2 pretreatment on cerium(IV) oxide (CeO_2) could result in an enrichment of Ce^{3+} on the sample surface, which leads to an increased content of active surface oxygen and strong-acid site production in the sample; these effects benefit SCR activity. Rivas et al. [24] reported that DCE-removal temperatures are lowered considerably by 80 °C (temperature for 50% reactant conversion, T_{50}) and 120 °C (temperature for 90% conversion, T_{90}) over a sulfated $Ce_{0.5}Zr_{0.5}O_2$ catalyst, which is associated with an increased total acidity and new Brönsted acid sites. Burch et al. [25] and Corro et al. [26] reported that the propane oxidation activity of Pt/Al_2O_3 was promoted by presulfation, and they ascribed this response to the interaction of surface sulfates with highly oxidized surface Pt atoms at the edge of the Pt particles. The effects of sulfation on the state of Pt that is supported on ceria-zirconia mixed oxides and the activity for hydrocarbon oxidation were also investigated. Weng's group [28,29] proposed that some more active sites are generated at the platinum-sulfate interface.

Several mechanisms for sulfur deactivation have been summarized in the literature [30–32], including: (1) a Pt crystal structure rearrangement, (2) electronic effects caused by sulfur, (3) the formation of surface Pt sulfate, (4) the formation of sulfate on the support or Pt/support interface, and (5) modification of Pt-CO bonding. According to Datta et al. [33], SO_2 adsorption onto γ-Al_2O_3 occurs initially at Lewis acid sites. Hamzehlouyan et al. [22] observed that Pt promotes surface sulfate formation, and thereby blocks sites where carbon monoxide is adsorbed preferentially. However, these processes require direct Pt-catalyst treatment in a SO_2 atmosphere, and research on support sulfation effect on Pt-based catalysts is limited.

This work focuses on the support sulfation (Ce-Zr-SO_4^{2-}) effect and aims to investigate the effect of SO_4^{2-} on the low-temperature catalytic activity of Pt/Ce-Zr-SO_4^{2-} and evaluate the effect of support sulfation on the SO_2-poisoning resistance.

2. Experimental

2.1. Catalyst preparation

A Ce-Zr support with a cerium to zirconium mole ratio of 4:1 was prepared by co-precipitation. Cerium(III) nitrate hexahydrate ($Ce(NO_3)_3{\cdot}6H_2O$) and zirconium nitrate trihydrate ($Zr(NO_3)_4{\cdot}3H_2O$) were dissolved in deionized water. An excess NaOH solution (1 mol/L) was added slowly while stirring via a peristaltic pump to the Ce-Zr solution. The pH was adjusted to above 10. The precipitate was centrifuged, washed, filtered, dried overnight at 110 °C, and calcined at 500 °C for 3 h. The synthesized sample was labeled CZ.

Ce-Zr-SO_4^{2-} supports different sulfuric acid mass fractions (0.5, 5, 10, and 15) wt% by wetness impregnation using an aqueous solution of sulfuric acid (H_2SO_4). CZs (3 g) were added into the mixture of H_2SO_4 solution (0.1 mol/L; 1.5, 15, 30, and 45 mL) and deionized water (48.5, 35, 20, and 5 mL). These solutions were impregnated uniformly by slow removal of water using a rotary evaporator at 70 °C. The resulting samples were dried overnight at 110 °C, calcined at 500 °C for 3 h, and labeled CZ-*x*S, where *x* represents the mass percentage of sulfate over the support.

The CZ-*x*S were loaded with 1 wt% Pt by wetness impregnation and water removal by using a rotary evaporator at 70 °C, in which chloroplatinic acid (H_2PtCl_6) solution was used as a Pt precursor. The catalysts were dried at 110 °C and calcined at 500 °C for 3 h. Finally, Pt/CZ, Pt/CZ-0.5S, Pt/CZ-5S, Pt/CZ-10S, and Pt/CZ-15S were obtained.

Pt/CZ-*x*S-B (*x* = 0.5, 5, 10, 15; B = sulfate loaded behind Pt) were prepared by using the same process as that for CZ-*x*S, except that Pt/CZ was used instead of CZ.

2.2. Characterization

Specific surface areas of catalysts were measured using the Brunauer-Emmett-Teller (BET) method from nitrogen adsorption isotherms. Experiments were conducted on an ASAP 2020 instrument (Micromeritics) at –196 °C. Prior to the experiments, samples were degassed at 200 °C for 4 h.

X-ray diffraction (XRD) patterns of the samples were recorded on an X' Pert Pro diffractometer with Cu K_α (λ = 0.154056 nm, 40 kV, 30 mA) radiation. The measurements were conducted in the 2θ range of 10° to 100° with a step size of 0.033°.

Temperature-programmed reduction with hydrogen (H_2-TPR) was performed on a FINE SORB-3010 E instrument. The sample (200 mg) was placed in a quartz reactor, pretreated in highly pure Ar at 200 °C for 2 h, and then cooled to 60 °C. The reducing gas used in all experiments was 5% H_2/95% Ar. The temperature was increased from 60 °C to 900 °C at 10 °C/min. The flow rates were 30 mL/min. A TCD detector was used at the reactor outlet to measure the hydrogen volume that was consumed during reduction.

Temperature-programmed desorption of CO (CO-TPD) was investigated on a FINE SORB-3010 E instrument. The sample (100 mg) was placed in a quartz reactor, pretreated in 5% H_2/Ar at 300 °C for 1 h, and then cooled to 30 °C in a He flow. CO adsorption was performed by admitting a flow of 5% CO/95% N_2 at 30 °C for 1.5 h. The sample was exposed to He for 1 h at 100 °C to remove reversibly and physically bound CO from the surface. Finally, desorption was carried out from 100 °C to 500 °C at 5 °C/min in a He stream. The flow rates were 30 mL/min. A TCD detector was used at the reactor outlet to measure the CO volume during desorption.

Temperature-programmed desorption of ammonia (NH_3-TPD) was conducted on a FINE SORB-3010E instrument. The sample (100 mg) was placed in a quartz reactor, pretreated in

He at 400 °C for 2 h and cooled to 50 °C. Ammonia adsorption was performed by admitting a flow of 1% NH_3/99% N_2 at 50 °C for 1.5 h. Subsequently, samples were exposed to He for 1 h at 100 °C to remove reversibly and physically bound ammonia from the surface. Finally, desorption was carried out from 100 to 550 °C at 5 °C/min in a He stream. The flow rates were 30 mL/min. A TCD detector was used at the reactor outlet to measure the volume of ammonia during desorption.

X-ray photoelectron spectroscopy (XPS) data were obtained by using an ESCALab 220i-XL electron spectrometer from VG Scientific using 300 W Al K_α radiation. The base pressure was ~3×10^{-7} Pa. Binding energies were referenced to the C 1*s* line at 284.6 eV from adventitious carbon.

Infrared spectra were examined by using Fourier transform infrared (FTIR) spectroscopy (Vertex 70, scan rate = 32 s^{-1}, resolution = 2.5 cm^{-1}) equipped with an MCT detector after pyridine adsorption (FTIR-pyridine). The powders were pressed into self-supporting disks (20 mg, 13 mm diameter). The sample cell was pretreated in N_2 at 400 °C for 30 min. The sample spectrum was recorded after cooling to room temperature. Then, the sample was exposed to 5 μL of pyridine for 30 min. Spectra were recorded after being purged with N_2 for a further 30 min at 150 °C to remove physisorbed pyridine.

2.3. Catalytic activity test

The catalytic activity was evaluated in a fixed-bed continuous reactor packed with 0.5 g catalyst and 1.5 g quartz sand. Complete oxidations of C_3H_6 and CO over the catalysts were conducted in a stream of simulated diesel exhaust. The feed (0.1% CO, 0.05% NO, 0.05% C_3H_6, 10% O_2, and N_2 balance) was introduced to the catalyst at 200 mL/min. To study the poisoning effect of SO_2 on the catalysts, 0.02% SO_2 was added to the simulated diesel exhaust stream. The total flow rate remained unchanged. The effluent gas was analyzed using an online FTIR spectrophotometer (VERTEX 70, Bruker, Germany) equipped with a multiple reflection transmission cell (Infrared Analysis Inc., with a 10.0-m path length). All spectra were taken at a resolution of 2.5 cm^{-1} for 32 scans. A curve of the relationship between the conversion and temperature was obtained in the light-off experiment.

3. Results and discussion

3.1. Catalyst characterization

3.1.1. Surface structure and composition

To clarify the connection between changes in catalytic activity and those of the surface structure/composition of fresh and sulfate samples before they were subjected to catalytic activity experiments, catalysts were studied by XRD to identify their crystal structures. Fig. 1 presents the XRD patterns of pure $CeZrO_2$ phases (PDF #02-1311) for both samples. Extra peaks were not ascribed to the presence of S-containing phases, and structural changes were not found in the Pt/CZ-10S. Sulfated species may have existed as surface or amorphous bulk species, such as hydrated surface sulfates or hydrogen sulfate species [24,34]. Pt species do not have a significant diffraction peak, which indicates that a high dispersion of Pt on the catalyst surface was below the XRD detection limit [13,14]. Crystallite sizes from XRD and BET surface area analyses of catalysts are summarized in Table 1. The Pt/CZ-10S crystallite size was 16.9 nm, which is larger than Pt/CZ. The increase in crystallite size could be attributed to the longer calcination time, because the Pt/CZ catalyst was heat treated at 500 °C for 6 h, whereas the Pt/CZ-10S catalyst was calcined at 500 °C for 9 h (SO_4^{2-} doping prolonged the process by 3 h), and/or the chemical sintering induced by the strong acid [24]. In addition, BET analysis indicated that, with 10 wt% SO_4^{2-} doping, the surface area decreased from 57.2 to 23.8 m^2/g, because ceria-zirconia surface is covered by sulfates.

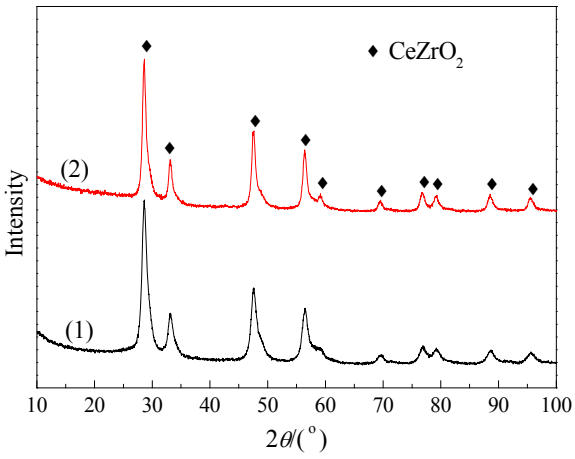

Fig. 1. XRD patterns of Pt/CZ (1) and Pt/CZ-10S (2) catalysts.

The amounts of Pt and sulfate groups on the Pt/CZ and Pt/CZ-10S surface were determined by XPS, and the results are listed in Table 1. As a type of surface-testing technology, XPS was used to test the depth distribution along the ~5–10 nm thickness [35]. The mass fraction of Pt on the Pt/CZ and Pt/CZ-10S surfaces were 2.88 wt% and 4.22 wt%, respectively. A comparison between the two fractions revealed that the mass fraction of Pt on the Pt/CZ-10S surface was greater than that of sample Pt/CZ, which indicates that support sulfation can improve the dispersion of Pt on the catalyst surface. The mass

Table 1
Some physico-chemical properties of Pt/CZ and Pt/CZ-10S catalysts.

Catalyst	Crystallite size (nm)	A_{BET} (m^2/g)	Element content [a]		Redox temperature for Pt (°C)	Pt dispersion [b] (%)
			Pt/support (%)	SO_4^{2-}/support (%)		
Pt/CZ	12.8	57.2	2.88	—	182	58
Pt/CZ-10S	16.9	23.8	4.22	10.64	141	85

[a] Measured by XPS. [b] Estimated from CO adsorption followed by TCD.

fraction of SO_4^{2-} on the Pt/CZ-10S surface after calcination at 500 °C for 6 h was 10.64 wt%, which indicates that most sulfate species remained after calcination at 500 °C.

3.1.2. Pt dispersion

Many metal-dispersion measurement methods exist, including the chemical adsorption method (static and dynamic), XPS, XRD, and transmission electron microscopy [36–39]. XPS results showed that the Pt dispersion increased after sulfation. Similar results were found for CO-TPD measurements in Fig. 2. The CZ sample did not release a detectable amount of CO between 100 and 500 °C at 5 °C/min, which demonstrates the importance of Pt nanoparticles in CO chemisorption. Under the same test conditions, two other Pt catalysts showed wide desorption peaks, which indicates some heterogeneity in the adsorption sites. This heterogeneity resulted from the different activation energies for desorption, which were a function of the surface coverage of CO on the Pt surface and depended on the Pt-particle size distribution [40]. Two CO desorption peaks can be differentiated, and CO desorption at low temperature (100–260 °C) was associated with linear CO adsorption over small Pt particles. CO desorption at high temperature (300–400 °C) can be ascribed to bridge-bonded CO species [41]. The Pt/CZ-10S catalyst also exhibited a wider CO desorption profile than the Pt/CZ catalyst, which implies a larger heterogeneity in metal particle-size distribution in the former. The adsorption stoichiometry of CO on Pt was 1:1, the amount of CO desorbed on the Pt/CZ catalyst corresponded to a platinum dispersion of 58%, and a platinum dispersion of 85% for the Pt/CZ-10S catalyst was obtained (Table 1). Torres et al. [42] reported that acidic sites have a strong interaction with H_2PtCI_6 during impregnation. When the CZ-S support was brought into contact with an aqueous solution of H_2PtCl_6, the increased acidic sites (Lewis and/or Brönsted, as shown in Fig. 4) on the sulfating supports would increase the Pt dispersion.

3.1.3. Redox properties

The reducibility of Pt species in supported Pt catalysts is an important factor and influences the catalytic oxidation performance. Redox properties of the catalysts are shown in Fig. 3,

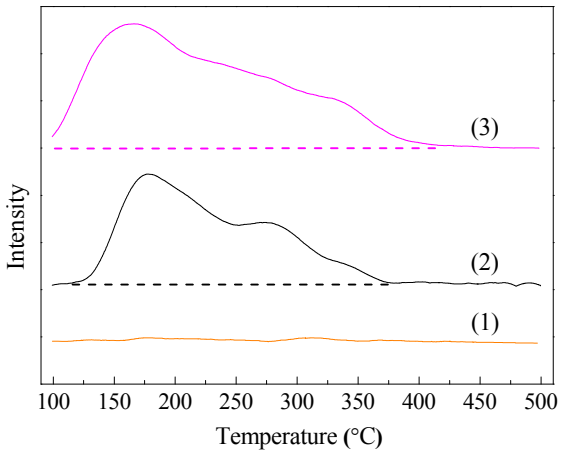

Fig. 2. CO-TPD profiles for CZ (1), Pt/CZ (2), and Pt/CZ-10S (3) samples.

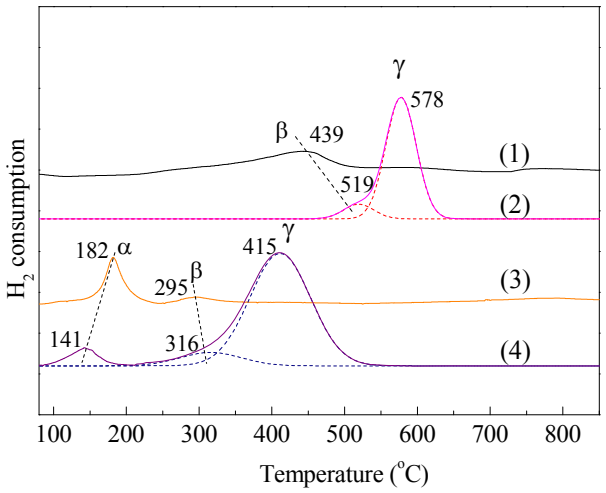

Fig. 3. H_2-TPR profiles for CZ (1), CZ-S (2), Pt/CZ (3), and Pt/CZ-10S (4) samples. (α) $PtO + H_2 \rightarrow Pt + H_2O$, $PtO_2 + 2H_2 \rightarrow Pt + 2H_2O$, $2CeO_{2\,(adjacent)} + H_2 \rightarrow Ce_2O_3 + H_2O$; (β) $2CeO_2 + H_2 \rightarrow Ce_2O_3 + H_2O$; (γ) $2SO_4^{2-} + 7H_2 \rightarrow SO_2 + H_2S + 6H_2O$.

and the reduction temperatures of the Pt species are listed in Table 1. A pure CZ sample displays a broad reduction peak that is centered at ~439 °C, which is attributed to Ce^{4+} reduction [43]. Two peaks exist in the reduction profiles of the CZS sample: one occurs at ~519 °C because of the reduction of Ce^{4+} to Ce^{3+}, and the other exists at ~578 °C because of the reduction in sulfated species to yield SO_2 and/or H_2S [44,45]. Ce^{4+} reduction and sulfated species are labeled as peaks β and γ, respectively. These two reduction processes make the interpretation of results from the H_2-TPR analysis more difficult. When evaluating H_2 uptake, differences in thermal conductivity between H_2 (170.64 mW m^{-1} K^{-1}), SO_2 (9.62 mW m^{-1} K^{-1}), H_2S (13.71 mW m^{-1} K^{-1}), and Ar (17.95 mW m^{-1} K^{-1}) [46] were assumed to be sufficiently large to prevent a major interference of SO_2 and H_2S formation and H_2 consumption. After loading Pt on the support, H_2 molecules were adsorbed and dissociated on Pt particles. H radicals that were created on a Pt surface would migrate to the support surface in a phenomenon termed "hydrogen spillover" [47]. Thus, CZ supports and S species could be reduced at lower temperature on Pt catalysts. The spillover effect of Pt for ceria-based oxides promotes the reduction of the adjacent ceria sites significantly. A uniform mass of Pt loadings yields a peak at a lower temperature in the Pt catalysts; this peak arose from the reduction of Pt species and adjacent ceria (labeled as peak α). As shown in Fig. 3, the Pt/CZ-10S sample had the lower reduction temperature for Pt of ~141 °C. Wang et al. [48] reported that the dispersion of active ingredients on the catalyst surface affects surface oxygen reduction significantly. In our previous work [2], H_2 was more easily activated with a higher Pt dispersion. Thus, we suppose that a good dispersion of Pt would result in good redox reactions of the catalysts.

3.1.4. Surface acidity

NH_3-TPD and FTIR-pyridine were used to evaluate the acidic properties of Pt/CZ and Pt/CZ-10S. Fig. 4 shows that after sulfation, the acid properties of the samples were affected no-

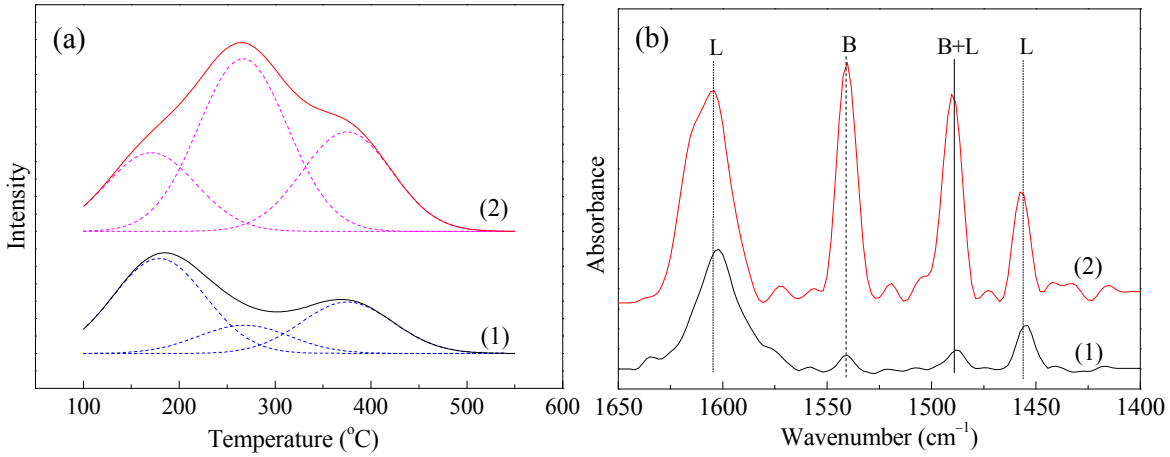

Fig. 4. NH_3-TPD profiles (a) and FTIR-pyridine difference spectra (b) for Pt/CZ (1) and Pt/CZ–10S (2) catalysts.

tably. The NH_3-TPD result was associated with an overall acidity and acid-strength distribution of catalysts. To establish the strength of these sites, desorption peaks were typically deconvoluted into three bands at ~175, 275, and 375 °C, which were correlated with a weak, moderate, and strong acidity, respectively [49]. The area under the TPD profiles gave an estimation of the amount of different acid sites in each sample, as listed in Table 2. As shown in Fig. 4(a) and Table 2, Pt/CZ showed a marked, broad low-temperature desorption peak at ~175 °C, which suggests that the acidic sites were mainly of weak acidity (> 50%). A notable enhancement of moderate and strong acidity resulted for the sulfated catalyst. Hence, the moderate and strong acidity of the Pt/CZ-10S increased from 10.5 and 18.9 μmol/g to 49.3 and 46.9 μmol/g, respectively. The overall acidity of the sulfated samples also increased from 64.4 μmol/g to 118.6 μmol/g.

FTIR spectroscopy of adsorbed pyridine is a useful technique that is used commonly for discernment of Brönsted and Lewis acid sites. The adsorbed pyridine probe molecules tend to couple with aprotic (Lewis) and/or protonic (Brönsted) catalytic centers through nitrogen lone-pair electrons, which can then be detected by monitoring the ring vibrations [50]. Some observations of the nature of acid sites on the samples were made through pyridine adsorption at 150 °C, followed by FTIR spectroscopy. The IR difference spectra within 1400–1650 cm^{-1} are shown in Fig. 4(b). In general, the band at 1540 cm^{-1} is assigned to Brönsted acid sites. Those at 1455 cm^{-1} and 1607 cm^{-1} can be assigned to Lewis acid sites; and that at 1490 cm^{-1} arose from a combination band that was associated with Brönsted and Lewis acid sites [35,50,51]. As shown in Fig. 4(b), Pt/CZ displayed only vibrational bands that belong to Lewis acid sites, and showed that Pt/CZ had no Brönsted acidity. In contrast, substantial differences resulted for the Pt/CZ-10S sample, i.e., a coexistence of Brönsted (at 1540 cm^{-1}) and Lewis (at 1455 and 1607 cm^{-1}) acidity, in addition to the combination band at 1495 cm^{-1}. Thus, new Brönsted acid sites were generated during the sulfation treatment of CZ. These results are consistent with those reported previously for sulfated ceria-zirconia catalysts obtained by Raman spectroscopy [24]. This increase can also be attributed to the elevated number of acid sites on the support surface, and in particular, to the new Brönsted acid sites.

Table 2
Acid properties for Pt/CZ and Pt/CZ–10S catalysts.

Catalyst	Acidity (μmol/g)			
	Weak	Moderate	Strong	Total
Pt/CZ	35.0 (54.4%)	10.5 (16.2%)	18.9 (29.4%)	64.4
Pt/CZ–10S	22.4 (18.9%)	49.3 (41.6%)	46.9 (39.5%)	118.6

3.1.5. XPS analysis

XPS was used to characterize changes in atomic binding energy and valence state after sulfation. XPS spectra of Pt 4*f* and O 1*s* on Pt/CZ and Pt/CZ-10S are shown in Fig. 5 and Table 3. Based on the XPS handbook [52], a Pt 4*f* band consisted of two parts that correspond to levels $4f_{7/2}$ (at low binding energy) and $4f_{5/2}$ (at high binding energy). The spacing between the Pt $4f_{7/2}$ and Pt $4f_{5/2}$ peak positions was 3.33. Two Pt $4f_{7/2}$ were found (Fig. 5(a)): the binding energy of Pt $4f_{7/2}$ at ~72.9 eV arose from the Pt^{2+} state, and the other at 75.1 eV arose from the Pt^{4+} state. As shown in Table 3, the relative content of Pt^{4+} increased, which indicates that the sulfating treatment led to an increase in highly oxidized surface Pt atoms (Pt^{4+}) on the Pt/CZ-10S catalyst. This could result from the polarization of these Pt atoms at the close proximity sites of the electronegative sulfate (SO_4^{2-}), which confers on the Pt atoms at the perimeter a more partial positive charge. Moreover, Burch et al. [25] proposed that the interaction of surface sulfates with highly oxidized Pt atoms at the edge of the Pt particles may constitute very active new catalytic sites ($Pt^{\&+}$-$(SO_4^{2-})^{\&-}$ couple), which leads to the enhanced activity that is observed on propane combustion.

Fig. 5(b) revealed the O 1*s* peaks for lattice oxygen O_α (529.6–530.0 eV), chemisorbed oxygen O_β (531.3–531.7 eV), and hydroxyl groups O_γ (532.7–533.5 eV) [53]. As shown in Table 3, the chemisorbed-oxygen content increased significantly after sulfation treatment, and was in good agreement with previous results on a sulfated CeO_2 sample [23]. The surface-adsorbed oxygen of the catalyst is the most active oxygen

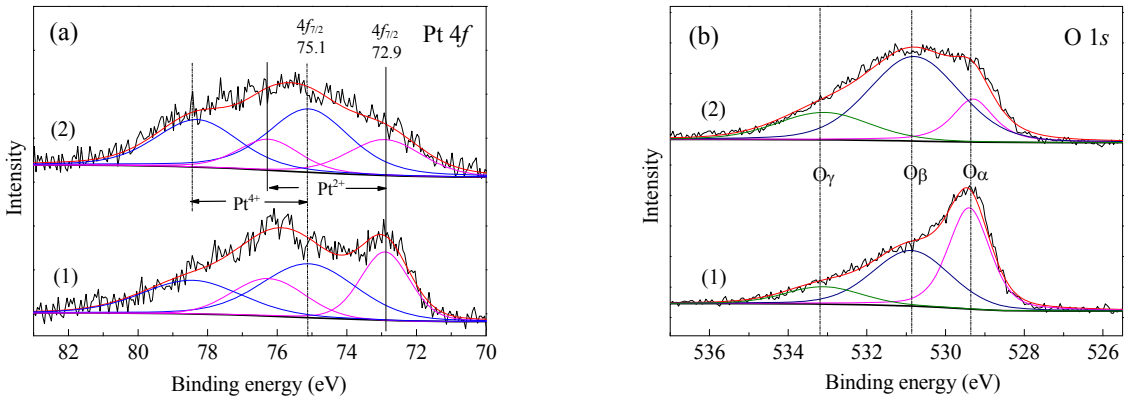

Fig. 5. XPS spectra of Pt/CZ (1) and Pt/CZ–10S (2). (a) Pt 4*f*; (b) O 1*s*.

in the redox reactions, and an increase in this oxygen is beneficial for oxidation efficiency.

Table 3
Percentages of various Pt 4*f* and O 1*s* on Pt/CZ and Pt/CZ-10S catalysts.

Catalyst	Relative concentration of Pt (%)		Relative concentration of O (%)		
	Pt^{2+}	Pt^{4+}	O_α	O_β	O_γ
Pt/CZ	39.8	60.2	45.2	41.9	12.9
Pt/CZ-10S	32.0	68.0	17.8	61.8	20.4

3.2. Catalytic activity and sulfur resistance

The oxidation of C_3H_6 and CO in the presence of simulated diesel exhaust was chosen as a measure to evaluate the impact of carrier sulfation on the Pt/Ce-Zr catalysts. Fig. 6 shows the differences in catalytic activity and sulfur resistance of Pt/CZ and Pt/CZ-10S. As shown in Fig. 6, Pt/CZ-10S exhibited a higher catalytic activity compared with Pt/CZ; the T_{50} of C_3H_6 and CO decreased by 36 and 49 °C, respectively. Carrier sulfation improved the low-temperature catalytic activity significantly. A remarkable decrease in C_3H_6 and CO oxidation activity of Pt/CZ catalyst was observed. We found that 0.02% SO_2 had a distinct poisoning effect on the C_3H_6 and CO conversion over the Pt/CZ sample, and that the additional increase of the T_{50} of C_3H_6 and CO was at least 20 °C. However, after carrier sulfation, only a slight decrease in C_3H_6 and CO conversion was observed when 0.02% SO_2 was added to the reaction gas, and the Pt/CZ-10S sample could reach 90% C_3H_6 and CO conversion at ~195 °C, with growth amounts below 10 °C. Moreover, the T_{50} of C_3H_6 and CO over the Pt/CZ-10S sample was roughly unchanged. Therefore, the catalyst had a strong resistance against SO_2 poisoning after loading with an appropriate amount of sulfate.

The stabilities of Pt/CZ and Pt/CZ-10S were investigated by analyzing the evolution of conversion with time on stream of 0.02% SO_2 at 240 °C for 20 h (Fig. 7(a)). The conversion of C_3H_6 and CO decreased after SO_2 addition to the Pt/CZ catalyst, i.e., the removal rate of C_3H_6 decreased from 83% to 56% with SO_2 addition during 20 h, and the decrease in CO removal rate was more obvious. After closing the SO_2 valve, the catalyst activity of Pt/CZ remained the same and did not return to its original level. Thus, Pt/CZ was deactivated by SO_2 poisoning. In addition, the Pt/CZ-10S catalyst was stable, with C_3H_6 and CO conversions of ~95% and 100%, respectively, throughout the entire simulation process.

Fig. 7(b) shows the Pt/CZ-10S that was investigated on a simulated stream at 180 °C for 96 h, which further verifies the ability of the sulfation catalyst for sulfur resistance and stability. This temperature was selected because it provided conversions of less than 100% over Pt/CZ-10S, which provided a more sensitive indication of changes in catalyst performance within the timeline. Results showed that conversions decreased after SO_2 addition, but that the catalyst activity was able to recover rapidly when SO_2 was removed. Thus, SO_2 had no poisonous effect on the Pt/CZ-10S catalyst, and the decrease in activities may result from the competitive adsorption relationship among C_3H_6, CO, and SO_2. In 12–36 h, the catalyst activity increased even in the presence of SO_2, with final conversion rates reaching 90% and 99% for C_3H_6 and CO, respectively, under SO_2-free condition. These high conversion rates were well retained, which is indicates that this high activity can be stable. These findings reveal that loading with an appropriate amount of sulfate could improve the catalytic performance and enable excellent stability and sulfur resistance under actual

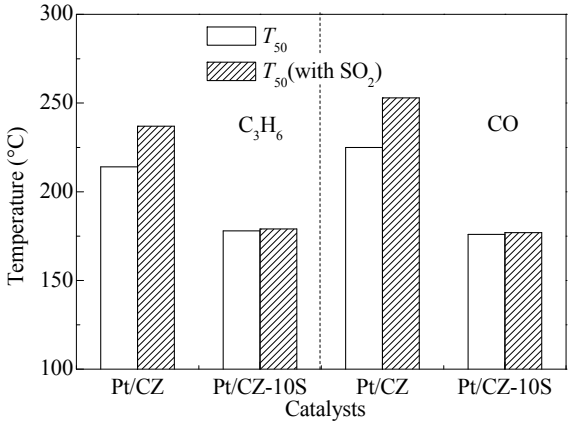

Fig. 6. Bar graph of T_{50} of C_3H_6 and CO for Pt/CZ and Pt/CZ–10S.

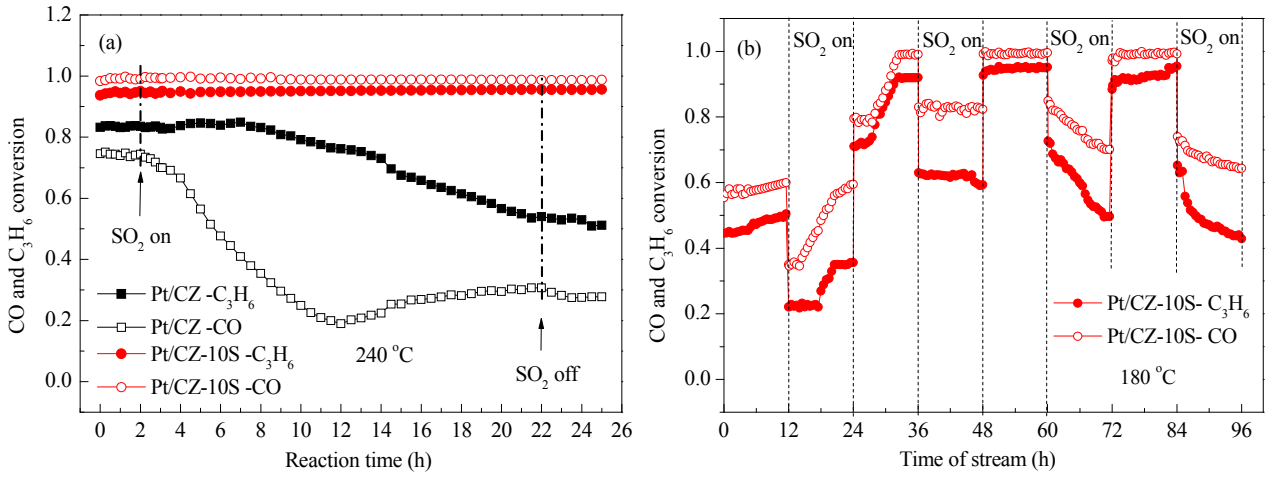

Fig. 7. Conversion rates of C_3H_6 (a) and CO (b) from a stream of simulated diesel exhaust catalyzed by Pt/CZ, Pt/CZ-10S.

operating conditions.

3.3. Discussion

To investigate the effect of SO_4^{2-} on the low-temperature catalytic activity and sulfur resistance of the Pt/Ce-Zr-SO_4^{2-} catalyst, Pt/CZ-S and Pt/CZ-S-B (B = sulfate loaded behind Pt) catalysts with various amounts of SO_4^{2-} were investigated in a simulated diesel exhaust (Fig. 8). The T_{50} and T_{90} over the catalysts are summarized in Table 4. Fig. 8(a) and (b) shows an increase in activity for all Pt/CZ-*x*S catalysts in the oxidation of C_3H_6 and CO in a simulated diesel exhaust, but this enhancement was not constant; the amount of SO_4^{2-} on the support also influenced the Pt/CZ-S catalyst performance. The Pt/CZ-5S catalyst exhibited the highest catalytic activity; further loading of sulfuric acid decreased the conversion for C_3H_6 and CO oxidation. Pt/CZ-S-B samples did not exhibit an improvement in activities as well as Pt/CZ-S (Fig. 8(c, d)), and among the

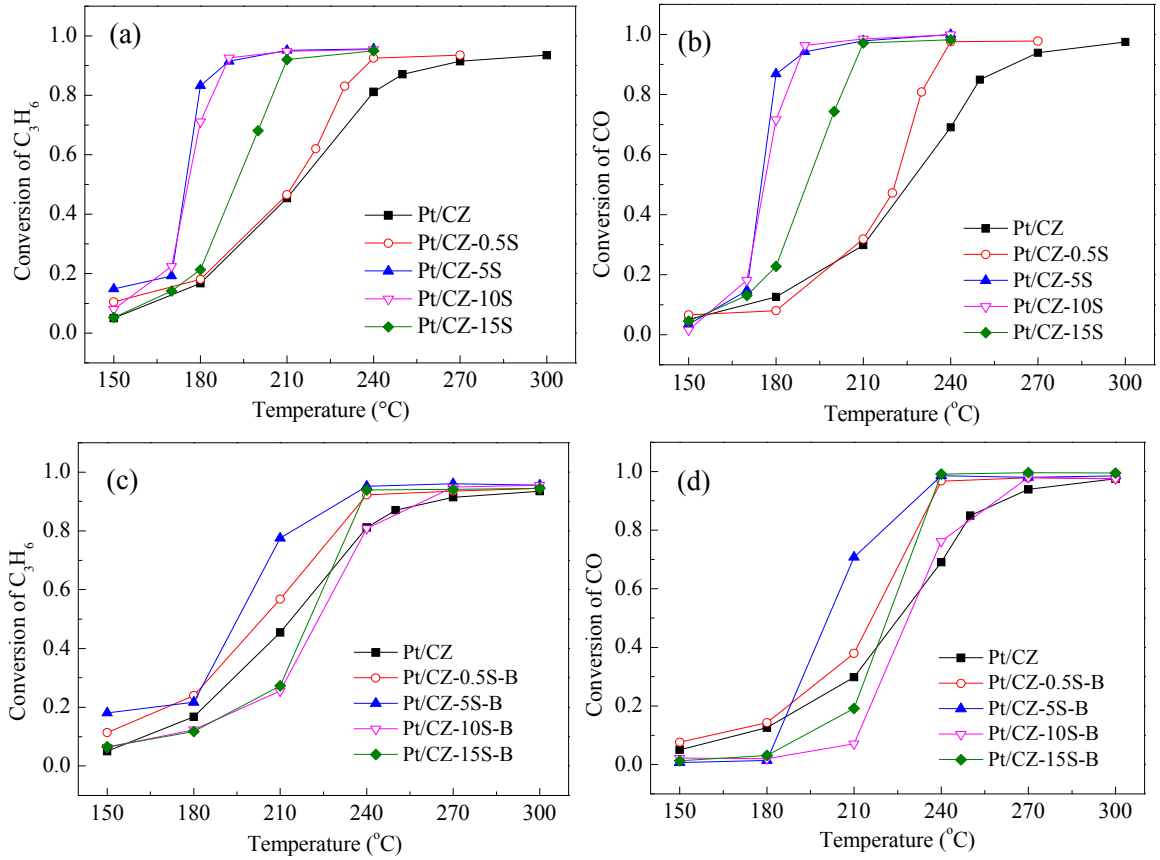

Fig. 8. Conversion rates of C_3H_6 (a) and CO (b) from a stream of simulated diesel exhaust without SO_2 catalyzed by Pt/CZ and Pt/CZ-*x*S; conversion rates of C_3H_6 (c) and CO (d) from a stream of simulated diesel exhaust catalyzed by Pt/CZ and Pt/CZ-*x*S-B.

Table 4
T_{50} and T_{90} of C_3H_6 and CO over Pt/CZ, Pt/CZ-*x*S and Pt/CZ-*x*S-B catalysts.

Catalyst	T_{50}/T_{90} (°C)		$\Delta T_{50}/\Delta T_{90}$ [a] (°C)	
	C_3H_6	CO	C_3H_6	CO
Pt/CZ	214/264	225/262	23/32	28/28
Pt/CZ-0.5S	212/237	221/235	—	—
Pt/CZ-5S	175/188	175/184	—	—
Pt/CZ-10S	178/188	176/187	1/10	1/6
Pt/CZ-15S	192/209	191/210	—	—
Pt/CZ-0.5S-B	204/238	216/237	—	—
Pt/CZ-5S-B	195/231	201/231	—	—
Pt/CZ-10S-B	223/260	229/259	1/5	1/3
Pt/CZ-15S-B	220/238	222/237	—	—

[a] ΔT_{50} (ΔT_{90}) = T_{50} (T_{90}) with 0.02% SO_2 – T_{50} (T_{90}) without SO_2.

Pt/CZ-*x*S-B catalysts, lower sulfate loadings exhibited a higher activity. Therefore, the existence of SO_4^{2-} is not the only factor that affects enhanced activity. Both catalysts exhibited an excellent sulfur resistance (as shown in Table 4).

With the series of characterization analyses in the former, we assume that these samples have the following characteristics: (1) the acidic properties of the Pt/CZ-S-B sample are similar to those of the Pt/CZ-S catalyst; (2) during sulfating treatment, the dispersion of Pt on Pt/CZ is unchanged, but the Pt particles are covered by sulfate species. The enhancement in low-temperature activity over Pt/CZ-*x*S could be attributed to an increased Pt dispersion and the synergetic catalysis of a $Pt^{\&+}$-$(SO_4^{2-})^{\&-}$ couple, including Pt particles and neighboring sulfate, and may be new active sites for the catalytic oxidation of C_3H_6 and CO on Pt/CZ-S. The improvement of sulfur resistance on the sulfated catalysts belongs to the increased acid sites.

4. Conclusions

Pt/CZ and Pt/CZ-S catalysts were prepared by wetness impregnation. For the sulfated catalyst, the crystalline structure over Pt/CZ-S did not show any appreciable changes, but the surface area decreased. As revealed by CO-TPD analysis, the presence of SO_4^{2-} on the support could improve the dispersion of Pt on the catalyst surface and the lower oxygen-reduction temperature on Pt was evaluated by H_2-TPR. The XPS measurements support the formation of a new active catalytic site ($Pt^{\&+}$-$(SO_4^{2-})^{\&-}$ couple), which consists of highly oxidized Pt atoms at the edge of the Pt particles and its neighboring sulfate. The addition of SO_4^{2-} increased the total acidity and the generation of new Brönsted acid sites on the Pt/CZ-S catalyst.

The combination of the results obtained from Pt/CZ, Pt/CZ-S, and Pt/CZ-S-B catalytic tests indicates that Pt/CZ-S exhibited the best catalytic activity for C_3H_6 and CO oxidation in a simulated diesel exhaust. The effects of SO_4^{2-} between Pt/CZ-S and Pt/CZ-S-B are different and could be ascribed to the notable enhancement of Pt dispersion on Pt/CZ-S catalyst and the buildup of more new active catalytic sites ($Pt^{\&+}$-$(SO_4^{2-})^{\&-}$ couple). The sulfur resistance of Pt/CZ-S and Pt/CZ-S-B were improved as a result of the increased total acidity and the new Brönsted acid sites on the sulfated catalysts.

References

[1] Y. D. Chen, L. Wang, X. X. Guan, S. H. Tang, M. C. Gong, Y. Q. Chen, *Chin. J. Catal.*, **2013**, 34, 667–673.
[2] H. F. Huang, B. Jiang, L. Gu, Z. H. Qi, H. F. Lu, *J. Environ. Sci.*, **2015**, 33, 135–142.
[3] C. L. Song, F. Bin, Z. M. Tao, F. C. Li, Q. F. Huang, *J. Hazard. Mater.*, **2009**, 166, 523–530.
[4] M. Khosravi, C. Sola, A. Abedi, R. E. Hayes, W. S. Epling, M. Votsmeier, *Appl. Catal. B*, **2014**, 147, 264–274.
[5] M. T. Cheng, H. J. Chen, L. H. Young, H. H. Yang, Y. I. Tsai, L. C. Wang, J. H. Lu, C. B. Chen, *J. Hazard. Mater.*, **2015**, 297, 234–240.
[6] K. Yamamoto, T. Sakai, *Catal. Today*, **2015**, 242, 357–362.
[7] V. Bermúdez, J. R. Serrano, P. Piqueras, O. García-Afonso, *Appl. Energy*, **2015**, 140, 234–245.
[8] S. Cimino, L. Lisi, M. Tortorelli, *Chem. Eng. J.*, **2016**, 283, 223–230.
[9] Z. B. Xiong, C. Wu, Q. Hu, Y. Z. Wang, J. Jin, C. M. Lu, D. X. Guo, *Chem. Eng. J.*, **2016**, 286, 459–466.
[10] M. Haneda, K. Suzuki, M. Sasaki, H. Hamada, M. Ozawa, *Appl. Catal. A*, **2014**, 475, 109–115.
[11] R. Raj, M. P. Harold, V. Balakotaiah, *Chem. Eng. J.*, **2015**, 281, 322–333.
[12] T. Kolli, M. Huuhtanen, T. Kanerva, M. Vippola, K. Kallinen, T. Kinnunen, T. Lepistö, J. Lahtinen, R. L. Keiski, *Top. Catal.*, **2011**, 54, 1185–1189.
[13] X. D. Wu, L. Zhang, D. Weng, S. Liu, Z. C. Si, J. Fan, *J. Hazard. Mater.*, **2012**, 225–226, 146–154.
[14] D. Y. Yoon, E. Lim, Y. J. Kim, J. H. Kim, T. Ryu, S. Lee, B. K. Cho, I. S. Nam, J. W. Choung, S. Yoo, *J. Catal.*, **2014**, 319, 182–193.
[15] M. M. Azis, X. Auvray, L. Olsson, D. Creaser, *Appl. Catal. B*, **2015**, 179, 542–550.
[16] N. Kamiuchi, M. Haneda, M. Ozawa, *Catal. Today*, **2013**, 201, 79–84.
[17] K. Hauff, U. Tuttlies, G. Eigenberger, U. Nieken, *Appl. Catal. B*, **2012**, 123–124, 107–116.
[18] F. Diehl, J. Barbier. Jr, D. Duprez, I. Guibard, G. Mabilon, *Appl. Catal. B*, **2010**, 95, 217–227.
[19] C. A. Neyertz, E. D. Banús, E. E. Miró, C. A. Querini, *Chem. Eng. J.*, **2014**, 248, 394–405.
[20] Y. Nagai, T. Hirabayashi, K. Dohmae, N. Takagi, T. Minami, H. Shinjoh, S. I. Matsumoto, *J. Catal.*, **2006**, 242, 103–109.
[21] Y. Zheng, Y. Zheng, Y. H. Xiao, G. H. Cai, K. M. Wei, *Catal. Commun.*, **2013**, 39, 1–4.
[22] T. Hamzehlouyan, C. S. Sampara, J. H. Li, A. Kumar, W. S. Epling, *Appl. Catal. B*, **2016**, 181, 587–598.
[23] T. T. Gu, Y. Liu, X. L. Weng, H. Q. Wang, Z. B. Wu, *Catal. Commun.*, **2010**, 12, 310–313.
[24] B. de Rivas, C. Sampedro, M. García-Real, R. López-Fonseca, J. I. Gutiérrez-Ortiz, *Appl. Catal. B*, **2013**, 129, 225–235.
[25] R. Burch, E. Halpin, M. Hayes, K. Ruth, J. A. Sullivan, *Appl. Catal. B*, **1998**, 19, 199–207.
[26] G. Corro, J. L. G. Fierro, V. C. Odilon, *Catal. Commun.*, **2003**, 4, 371–376.
[27] G. Corro, C. Cano, J. L. G. Fierro, *Catal. Commun.*, **2008**, 9, 2601–2605.
[28] B. Wang, X. D. Wu, R. Ran, Z. C. Si, D. Weng, *J. Mol. Catal. A*, **2012**, 361–362, 98–103.
[29] L. Zhang, D. Weng, B. Wang, X. D. Wu, *Catal. Commun.*, **2010**, 11, 1229–1232.

Graphical Abstract

Chin. J. Catal., 2017, 38: 607–616 doi: 10.1016/S1872-2067(17)62781-5

Propene and CO oxidation on Pt/Ce-Zr-SO_4^{2-} diesel oxidation catalysts: Effect of sulfate on activity and stability

Lei Gu, Xiao Chen, Ying Zhou, Qiulian Zhu, Haifeng Huang *, Hanfeng Lu *
Zhejiang University of Technology

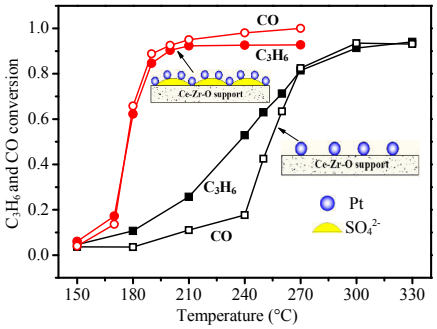

Support sulfation improved catalytic activity and sulfur resistance of Pt/Ce-Zr-SO_4^{2-} catalyst significantly, as their Pt dispersity and total acidity increased, and new active sites ($Pt^{\&+}$-$(SO_4^{2-})^{\&-}$ couples) were generated.

[30] F. J. Gracia, S. Guerrero, E. E. Wolf, J. T. Miller, A. J. Kropf, *J. Catal.*, **2005**, 233, 372–387.
[31] J. H. Pazmiño, J. T. Miller, S. S. Mulla, W. N. Delgass, F. H. Ribeiro, *J. Catal.*, **2011**, 282, 13–24.
[32] Y. S. Kim, S. J. Lim, Y. H. Kim, J. H. Lee, H. I. Lee, *Res. Chem. Intermed.*, **2012**, 38, 947–955.
[33] A. Datta, R. G. Cavell, R. W. Tower, Z. M. George, *J. Phys. Chem.*, **1985**, 89, 443–449.
[34] B. Azambre, L. Zenboury, J. V. Weber, *P. Burg, Appl. Surf. Sci.*, **2010**, 256, 4570–4581.
[35] A. Torrisi, *Appl. Surf. Sci.*, **2008**, 254, 2650–2658.
[36] H. Zhang, X. J. Liu, N. W. Zhang, J. B. Zheng, Y. P. Zheng, Y. H. Li, C. J. Zhong, B. H. Chen, *Appl. Catal. B*, **2016**, 180, 237–245.
[37] E. O. Jardim, S. Rico-Francés, F. Coloma, J. A. Anderson, J. Silvestre-Albero, A. Sepúlveda-Escribano, *J. Colloid Interface Sci.*, **2015**, 443, 45–55.
[38] Y. Wang, H. H. Liu, S. Y. Wang, M. F. Luo, J. Q. Lu, *J. Catal.*, **2014**, 311, 314–324.
[39] A. V. Rosario, E. C. Pereira, *Appl. Catal. B*, **2014**, 144, 840–845.
[40] P. Thormählen, M. Skoglundh, E. Fridell, B. Andersson, *J. Catal.*, **1999**, 188, 300–310.
[41] R. Padilla, M. Benito, L. Rodríguez, A. Serrano-Lotina, L. Daza, *J. Power Sources*, **2009**, 192, 114–119.
[42] G. C. Torres, E. L. Jablonski, G. T. Baronetti, A. A. Castro, S. R. de Miguel, O. A. Scelza, M. D. Blanco, M. A. Peña Jiménez, J. L. G. Fierro, *Appl. Catal. A*, **1997**, 161, 213–226.
[43] N. Kamiuchi, M. Haneda, M. Ozawa, *Catal. Today*, **2014**, 232, 179–184.
[44] H. Y. Zhao, S. Bennici, J. X. Cai, J. Y. Shen, A. Auroux, *J. Catal.*, **2010**, 274, 259–272.
[45] P. Bazin, O. Saur, F. C. Meunier, M. Daturi, J. C. Lavalley, A. M. Le Govic, V. Harlé, G. Blanchard, *Appl. Catal. B*, **2009**, 90, 368–379.
[46] C. L. Yaws, *Matheson Gas Data Book*, 7th ed., McGraw-Hill & Matheson Tri-Gas, Parsippany, **2001**.
[47] R. Prins, *Chem. Rev.*, **2012**, 112, 2714–2738.
[48] G. Wang, R. You, M. Meng, *Fuel*, **2013**, 103, 799–804.
[49] L. Matejová, P. Topka, L. Kaluža, S. Pitkäaho, S. Ojala, J. Gaálová, R. L. Keiski, *Appl. Catal. B*, **2013**, 142–143, 54–64.
[50] W. H. Chen, H. H. Ko, A. Sakthivel, S. J. Huang, S. H. Liu, A. Y. Lo, T. C. Tsai, S. B. Liu, *Catal. Today*, **2006**, 116, 111–120.
[51] M. I. Zaki, A. A. M. Ali, *Colloids Surf. A*, **1996**, 119, 39–50.
[52] J. F. Moulder, W. F. Stickle, P. E. Sobol, K. D. Bomben, *Handbook of X-Ray Photoelectron Spectroscopy*, Perkin-Elmer Corp., Eden Prarie, MN, USA, **1992**.
[53] M. Kang, E. D. Park, J. M. Kim, J. E. Yie, *Appl. Catal. A*, **2007**, 327, 261–269

Page numbers refer to the contents in the print version, which include both the English version and extended Chinese abstract of the paper. The online version only has the English version. The pages with the extended Chinese abstract are only available in the print version.